

3 Metallurgical aspects of welding

3.1 The temperature cycle

During welding, the material to be welded experiences a thermal cycle: the material is heated rapidly and cools down at a somewhat slower rate. When discussing this thermal cycle a distinction should be made between fusion welding and solid state welding. In the case of fusion welding the maximum temperature exceeds locally the melting point and a weld pool is formed, while the unmolten material reaches a maximum temperature, which depends on the distance from the fusion boundary. During the cooling phase of the welding process the liquid weld metal solidifies again, forming the weld. In the case of solid state welding the situation is less complicated as no melting occurs. However, in both cases the temperature cycle strongly influences the structure and the properties of the material. Particularly, the peak temperature (the maximum temperature reached) and the cooling rate play an important role.

As the starting point for a further discussion of the temperature cycle, we consider the simple case of a linear bead-on-plate weld produced by arc welding. The situation is shown schematically in Figure 3.1. The temperature in the plate is a function of time and position, and the temperature distribution can therefore be displayed in different ways. Figure 3.2 shows the temperature as a function of time for different locations in the plate, while Figure 3.3 shows the temperature as a function of the x - and y -coordinates at a given time. Figure 3.4 shows the isotherms at the surface of the plate and in a cross-section.

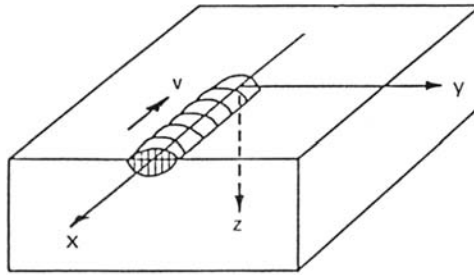


Figure 3.1. Schematic representation of a bead-on-plate weld and the coordinate system (v is the travel speed).

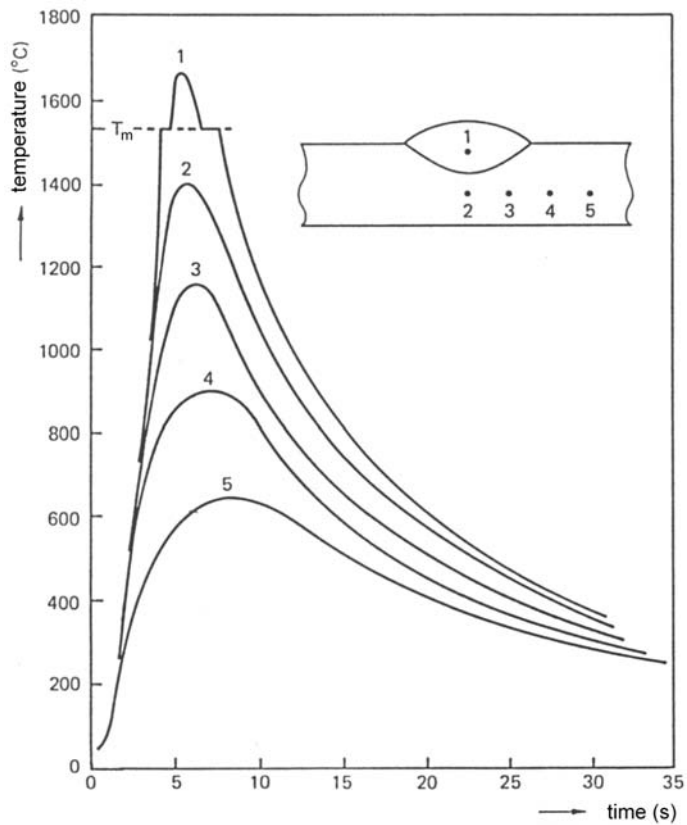


Figure 3.2. Temperature as a function of time for different locations in the plate (T_m is the melting temperature).

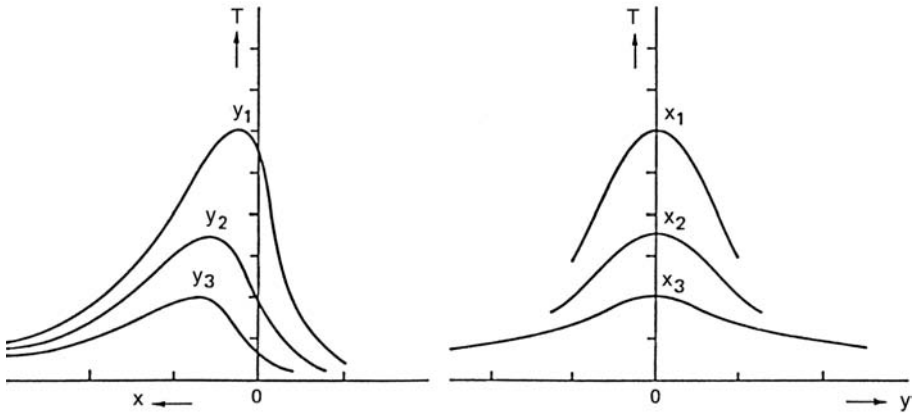


Figure 3.3. Temperature as a function of the x- and y- coordinates at a given time.

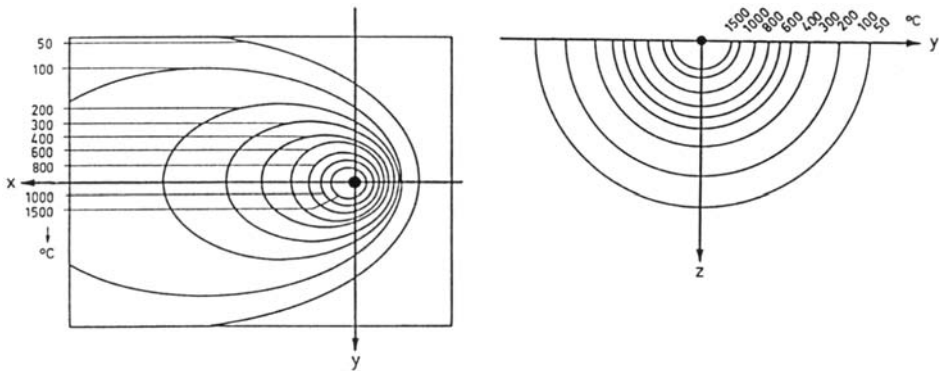


Figure 3.4. Isotherms at the surface of the plate and in a cross-section.

The temperature distribution in the plate during welding can be calculated using the law of conservation of energy. This yields for the case described:

$$\rho c \frac{\partial T}{\partial t} = \nabla \cdot (k \nabla T) - \rho c v \nabla T + q \quad (3.1)$$

For the meaning of the symbols used in this section, see Table 3.1.

In the case of a travelling coordinate system (the origin of the coordinate system travels along with the arc), a stationary situation exists with $\partial T / \partial t = 0$. Equation (3.1) can now be rewritten as:

$$\nabla \cdot (k \nabla T) - \rho c v \frac{\partial T}{\partial x} + q = 0 \quad (3.2)$$

Table 3.1. Meaning of the symbols used.

Symbol	Meaning
x, y, z	coordinates of space
$R = \sqrt{x^2 + y^2 + z^2}$	distance to the heat source
$r = \sqrt{y^2 + z^2}$	distance to the centre of the weld
t	time
$T(t, r)$	temperature as function of time and location
T_0	initial temperature of the plate
T_p	peak temperature
k	coefficient of thermal conductivity
c	specific heat
ρ	density
$\alpha = k/\rho c$	thermal diffusivity
q	heat produced per unit of volume
K_0	Bessel function of the 2nd kind and the 0 th order
Q	heating power ($\eta_p V I$ for arc welding)
η_p	process efficiency
V	arc voltage
I	welding current
v	travel speed
$W = Q/v$	heat input
d	plate thickness

To enable solving this equation analytically, the following simplifications are assumed:

- the heat source is concentrated in one point and has an infinite temperature;
- the physical properties of the metal are independent of temperature;
- no heat exchange occurs between the plate and the environment;
- the plate is flat and has large dimensions;
- latent heat of fusion is ignored.

Taking these simplifications into account, equation (3.2) can now be written for the region outside the heat source ($q = 0$) as:

$$\frac{k}{\rho c} \left(\frac{\partial^2 T}{\partial x^2} + \frac{\partial^2 T}{\partial y^2} + \frac{\partial^2 T}{\partial z^2} \right) - v \frac{\partial T}{\partial x} = 0 \quad (3.3)$$

Equation (3.3) can be solved for the case of two-dimensional heat flow (2-D) and for the case of three-dimensional heat flow (3-D). The two situations are shown schematically in Figure 3.5.

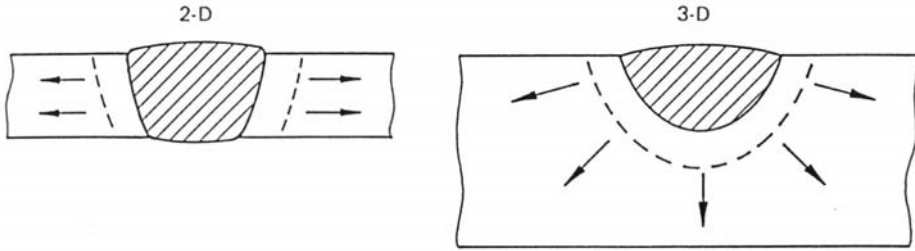


Figure 3.5. Schematic representation of two-dimensional (2-D) and three-dimensional (3-D) heat flow.

The solutions of equation (3.3) can be written as:

$$\text{2-D:} \quad T - T_0 = \frac{Wv}{2\pi kd} K_0 \left(\frac{vR}{2\alpha} \right) \exp \left(\frac{vx}{2\alpha} \right) \quad (3.4a)$$

$$\text{3-D:} \quad T - T_0 = \frac{Wv}{2\pi kR} \exp \left(-\frac{v(R-x)}{2\alpha} \right) \quad (3.4b)$$

From these equations, the temperature cycle experienced by a specific volume element of the material can be calculated. By approximation this leads to:

$$\text{2-D:} \quad T(t, r) - T_0 = \frac{W}{2dk} \sqrt{\frac{\alpha}{\pi t}} \exp \left(-\frac{r^2}{4\alpha t} \right) \quad (3.5a)$$

$$\text{3-D:} \quad T(t, r) - T_0 = \frac{W}{2\pi kt} \exp \left(-\frac{r^2}{4\alpha t} \right) \quad (3.5b)$$

An expression for the peak temperature $T_p(r)$ can be obtained by differentiating equations (3.5a) and (3.5b) with respect to t and equalizing the results to zero. It then follows:

$$\text{2-D:} \quad T_p(r) - T_0 = \sqrt{\frac{1}{2\pi e}} \cdot \frac{\alpha W}{dkr} \quad (3.6a)$$

$$\text{3-D:} \quad T_p(r) - T_0 = \frac{2\alpha W}{\pi ekr^2} \quad (3.6b)$$

Equations (3.6a) and (3.6b) show that with increasing distance to the centre of the weld, the peak temperature decreases more rapidly in the case of a three-dimensional heat flow (proportional to $1/r^2$) than in the case of two-dimensional heat flow

(proportional to $1/r$). As a result, the heat-affected zone will be narrower in the case of a thick plate than in the case of a thin plate. Furthermore, the peak temperature (and therefore the width of the heat affected-zone) increases proportionally to the heat input in both cases.

For the cooling rate $\partial T/\partial t$, only simple equations for the centre of the weld ($r = 0$) exist; however, these equations are also approximately valid for the heat-affected zone:

$$\text{2-D:} \quad \frac{\partial T}{\partial t} = - \frac{2\pi k^2 d^2 (T - T_0)^3}{\alpha W^2} \quad (3.7a)$$

$$\text{3-D:} \quad \frac{\partial T}{\partial t} = - \frac{2\pi k (T - T_0)^2}{W} \quad (3.7b)$$

Equations (3.7a) and (3.7b) show that the influence of pre-heating (T_0) on the cooling rate is substantial, especially in the case of two-dimensional heat flow.

An important quantity in describing the changes in microstructure that occur when welding low-carbon steels, is the cooling time between 800 °C and 500 °C ($\Delta t_{8/5}$), see the iron-carbon phase diagram (Figure 4.2). It can be shown that this time is approximately the same for all locations in the heat-affected zone that have been heated above 900 °C. The value of $\Delta t_{8/5}$ may be calculated using equations (3.7a) and (3.7b), which results in:

$$\text{2-D:} \quad \Delta t_{8/5} = \frac{\alpha W^2}{4\pi k^2 d^2} \left\{ \left(\frac{1}{500 - T_0} \right)^2 - \left(\frac{1}{800 - T_0} \right)^2 \right\} \quad (3.8a)$$

$$\text{3-D:} \quad \Delta t_{8/5} = \frac{W}{2\pi k} \left\{ \frac{1}{500 - T_0} - \frac{1}{800 - T_0} \right\} \quad (3.8b)$$

To distinguish between a two-dimensional heat flow and a three-dimensional heat flow situation a critical plate thickness d_{cr} can be defined. The value of d_{cr} can be obtained by equalizing $\Delta t_{8/5}$ for both cases. This leads to:

$$d_{cr} = \sqrt{\frac{\alpha W}{2k} \left\{ \frac{1}{500 - T_0} + \frac{1}{800 - T_0} \right\}} \quad (3.9)$$

The equations derived in the foregoing are valid for the situation in which the heat source is moving along a straight line at constant speed with respect to the

workpiece. This is the situation occurring during most fusion welding processes such as arc welding, oxy-fuel gas welding and power beam welding.

When the heat source does not move with respect to the workpiece ($v = 0$), the basic heat flow equation (3.1) reduces for the region outside the heat source ($q = 0$) to:

$$\rho c \frac{\partial T}{\partial t} = \nabla \cdot (k \nabla T) \quad (3.10)$$

Equation (3.10) refers to the situation in which the welding heat Q is released instantaneously, i.e. in a theoretically infinitely small period of time. A distinction can be made between three different heat source types:

- point source: the heat is released in a point at the surface, such as in the case of a laser pulse or an arc strike (see Figure 3.6a);
- line source: the heat is released along a line of length l , such as in the case of a spot weld (see Figure 3.6b);
- plane source: the heat is released at a cross-section of surface area A in an extended rod, such as in the case of a flash-butt weld (see Figure 3.6c).

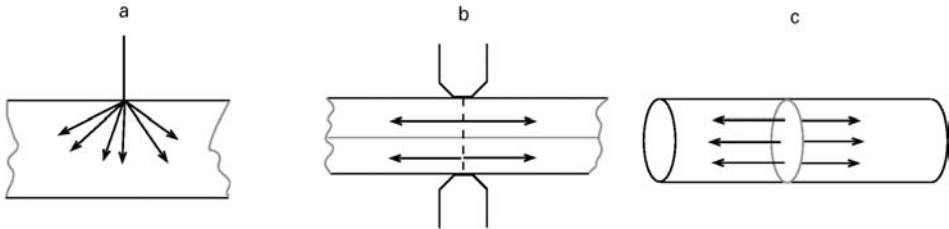


Figure 3.6. Heat flow in the case of:
a) point source, b) line source and c) plane source.

The solutions of equation (3.10) for the three heat sources can be written as:

$$\text{point source: } T(t, R) - T_0 = \frac{2Q}{\rho c (4\pi\alpha t)^{3/2}} \exp\left(-\frac{R^2}{4\alpha t}\right) \quad (3.11a)$$

$$\text{line source: } T(t, r) - T_0 = \frac{Q/l}{\rho c (4\pi\alpha t)} \exp\left(-\frac{r^2}{4\alpha t}\right) \quad (3.11b)$$

$$\text{plane source: } T(t, r) - T_0 = \frac{Q/A}{\rho c (4\pi\alpha t)^{1/2}} \exp\left(-\frac{r^2}{4\alpha t}\right) \quad (3.11c)$$

Equations (3.11a, b and c) describe the temperature distribution around the weld as function of time. From these equations, expressions for the peak temperature and the cooling rate as function of the distance to the weld can be obtained.

It must be noted that, due to the assumptions made, the equations derived in the foregoing are approximate in nature. They are, however, generally well applicable in practice.

More accurate results can be obtained by adequate modelling of the heat source. This allows for a wider variety of the heat transfer distribution to the workpiece. In this way the different welding processes can be addressed more accurately. For instance in laser welding a circular disk heat source is realistic, while for arc welding processes a Gaussian distribution or an ellipsoidal density heat source is more appropriate.

When a more precise description of the temperature cycle is required, numerical calculation methods such as the Finite Element Method (FEM) can be used. With numerical calculations it is possible to account for some variables that are not included in the analytical calculations, such as the temperature dependence of the material properties, the limited dimensions of the workpiece and the heat transfer from the material to the environment. However, it should be realized that also in the case of numerical calculations often assumptions are needed.

3.2 The weld pool

During fusion welding, part of the workpiece is melted, which results in the formation of a weld pool. When no consumable electrode or filler wire is used, the weld pool consists of molten parent metal. However, when using consumable material, the weld pool consists of a mixture of molten parent metal and molten consumable material. The composition of this mixture is determined by the mixing ratio M , which is defined as:

$$M = \frac{\text{weight of molten parent material}}{\text{total weight of molten material}} \times 100\% \quad (3.12)$$

The value of M depends on the welding process and on the welding parameters used.

The shape and size of the weld pool have an important influence on the microstructure of the solidified weld metal, due to the fact that during solidification the primary grains of the weld metal grow perpendicularly to the fusion boundary (see Section 3.5.1). Both shape and size of the weld pool depend strongly on the material properties (thermal conductivity, specific heat) and the welding parameters used. In particular the heating power and the travel speed play an important role. It is

obvious that with increasing heating power the width and the depth of the weld pool increase, whereas with increasing travel speed, the weld pool becomes more elongated: the shape changes from a circle (zero travel speed) via an ellipse to a tear shape.

In the case of power beam welding (plasma arc welding, laser welding and electron beam welding) a distinction should be made between two operating modes: the conduction mode and the keyhole mode, see Section 2.1.3.

In the weld pool, several physical and chemical phenomena may take place. Because of the relatively short lifespan of the weld pool, equilibrium situations are usually not reached.

An important phenomenon occurring in the weld pool is flow of the liquid metal. Due to its convective action, this flow will affect the shape and dimensions of the weld pool.

Usually, two different flow patterns are distinguished (Figure 3.7):

- radial outward directed flow, which leads to a relatively wide and shallow weld pool;
- downward directed flow, which results in a relatively narrow and deep weld pool.

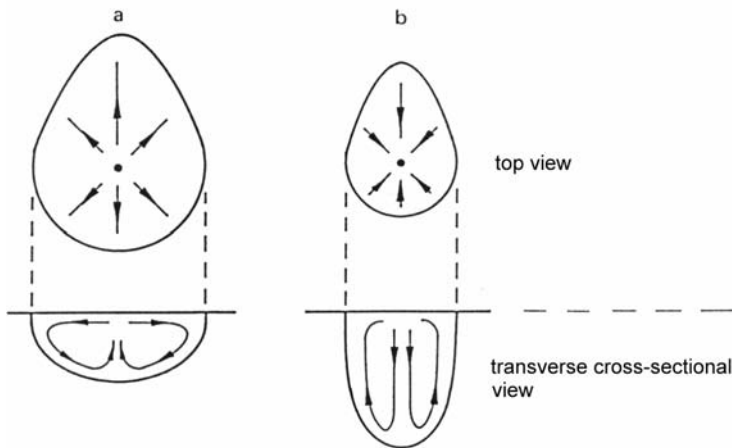


Figure 3.7. Flow patterns in the weld pool: a) radial outward directed flow; b) downward directed flow.

Extensive research has shown that fluid flow in the weld pool can be generated by different driving forces, the most important being forces due to variations in surface tension, electromagnetic forces, plasma drag and buoyancy.

– *Forces due to variation in surface tension*

The surface temperature of the weld pool will usually be maximum in the centre of the weld pool and decreases with increasing distance from the centre. In the case

of pure metals, the surface tension decreases with increasing temperature. This is indicated by line a in Figure 3.8. The negative gradient of the surface tension generates outward directed flow (Marangoni-flow). The resulting flow pattern is shown in Figure 3.7a.

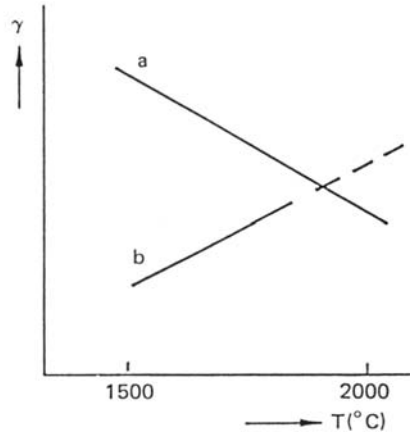


Figure 3.8. Surface tension as a function of temperature for iron a) without and b) with surface-active elements.

It has been shown that adding certain surface-active elements to a pure metal may lead to a reduction in surface tension and a reversal of the surface tension gradient (i.e. the surface tension does not decrease, but increases with increasing temperature (line b in Figure 3.8). This is, for instance, the case when sulfur, selenium or oxygen are added to pure iron. Under these conditions, a downward directed Marangoni-flow will develop (see Figure 3.7b).

– *Electromagnetic forces*

In the case of arc welding, electromagnetic (Lorentz-) forces are generated in the weld pool due to the divergence of the electric current. This divergence causes pressure differences in the weld pool, resulting in downward directed flow (Lorentz-flow). The resulting flow pattern is shown in Figure 3.7b.

– *Plasma drag*

During arc welding, a plasma flow is generated in the arc, which is directed from the electrode towards the weld pool (see Section 1.3). When reaching the surface of the weld pool, this plasma spreads out in radial direction along the surface of the weld pool, thus acting as a drag force, which results in outward directed flow (see Figure 3.7a).

– *Buoyancy*

The liquid metal in the weld pool has the lowest temperature and, hence, the highest density in the vicinity of the fusion boundary. This gives rise to a buoyancy force, which causes the liquid metal to move downward along the solidification front, resulting in outward directed flow (see Figure 3.7a).

It appears that of the driving forces, briefly described above, in most cases the last two are negligibly small and that only Marangoni-flow and Lorentz-flow should be considered. Which of the two dominates in a specific situation depends on the welding process, the welding parameters and the chemical composition of the weld metal. In most situations Marangoni-flow plays the dominant role. However, in the case of arc welding Lorentz-flow usually dominates the flow pattern.

In situations where Marangoni-flow is dominant, it is possible that the direction of the flow unexpectedly reverses due to variations in the concentration of surface-active elements (see above). As a result of these reversals, undesirable variations in penetration depth (cast-to-cast variations) may occur, as illustrated schematically in Figure 3.9. The variations in penetration depth form a serious problem, especially in the case of automated welding, where a welder cannot interfere to take corrective action.

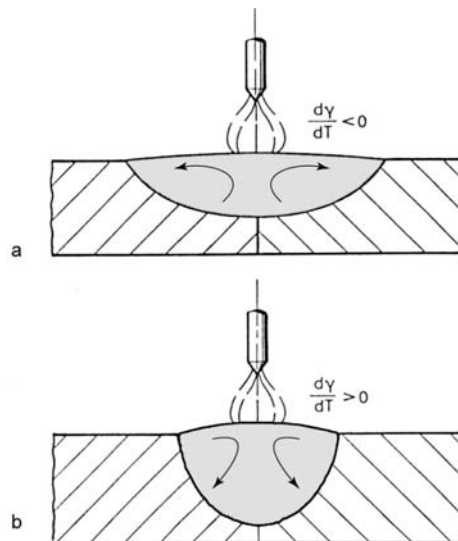


Figure 3.9. Influence of surface-active elements on weld pool geometry in the case of GTA welding of stainless steel: a) low concentration, $d\gamma/dT < 0$, outward flow, wide and shallow weld pool); b) high concentration, $d\gamma/dT > 0$, inward flow, narrow and deep weld pool.

It is obvious that in the case of welding with a consumable electrode, no regular flow pattern is observed due to the disturbing action of the impinging droplets.

3.3 Slag-weld pool reactions

In some welding processes slag is used with the aim to shield the molten metal (weld pool and droplet) from the surrounding atmosphere. This is for instance the case when welding steel with one of the variants of the arc welding process (such as SMA welding, GMA welding with flux-cored wire or SA welding – see Section 1.7). When slag is involved in the welding process, reactions may occur between the slag and the liquid metal. These reactions occur at the interface between the liquid slag and the liquid metal (droplet and/or weld pool) and are similar to the reactions taking place during the production of steel, except for the fact that in the case of welding they usually take place at a higher temperature and thus proceed much faster.

As an illustration, we consider the slag-metal reactions, which occur when welding carbon steel by means of the SMA welding process. In this case the slag, originating from the coating of the welding electrode, consists of oxides (mainly FeO, MnO and SiO₂).

The relevant reaction equations are:



In these reaction equations, the brackets around the reacting components indicate whether they are present in the [weld pool], in the (slag) or as {gas}.

The liquid steel contains carbon, which will react with the oxygen according to:



The reaction (3.16) leads to decarburisation of the weld metal, while the emerging CO may create porosity. Because the oxygen concentration [O] must have the same value for all four equilibrium equations, it follows that [Mn], [Si], [C], [O], and {CO} are unambiguously determined by the concentrations of (FeO), (MnO), and (SiO₂).

3.4 Absorption of di-atomic gases

During fusion welding of metals, di-atomic gases may be absorbed by the liquid weld metal from the surrounding atmosphere. The most important gases to be considered are oxygen, nitrogen and hydrogen (originating from water or hydrocarbons). Generally speaking, these gases have an unfavourable effect on the mechanical properties of the weld and for this reason strict precautions are usually taken to shield the weld pool from the surrounding by means of an inert gas or a slag.

Absorption of a di-atomic gas by a metal occurs in two steps. First, dissociation of the di-atomic molecules G_2 takes place at the surface of the metal:



Subsequently, (part of) the gas atoms $\{G\}$ are absorbed by the metal. This absorption process continues until equilibrium is reached between the inflow and outflow of gas atoms.

The concentration $[G]$ of the atomic gas that remains in solution under equilibrium conditions (the solubility S) depends on the temperature of the metal and the partial pressure p_{G_2} of the molecular gas G_2 in contact with the metal. The solubility is governed by Sieverts' law:

$$S = k \sqrt{p_{G_2}} \quad (3.18)$$

where k is a proportionality factor, which can be written as:

$$k = k_0 \exp -\Delta G / RT \quad (3.19)$$

with k_0 the solubility constant, ΔG the free energy of solution, R the gas constant and T the absolute temperature.

At high temperatures, the vapour pressure of the metal p_M should be taken into account and equation (3.18) takes the form:

$$S = k \sqrt{p_{G_2}(1 - p_M)} \quad (3.20)$$

The solubility S of a di-atomic gas at a given value of p_{G_2} as a function of temperature is schematically depicted in Figure 3.10.

The figure shows that, as predicted by equations (3.18) and (3.20), the solubility

- increases with temperature in the solid metal;
- increases abruptly at the melting point;
- increases further in the liquid metal;

- and starts to decrease upon approaching the boiling point.

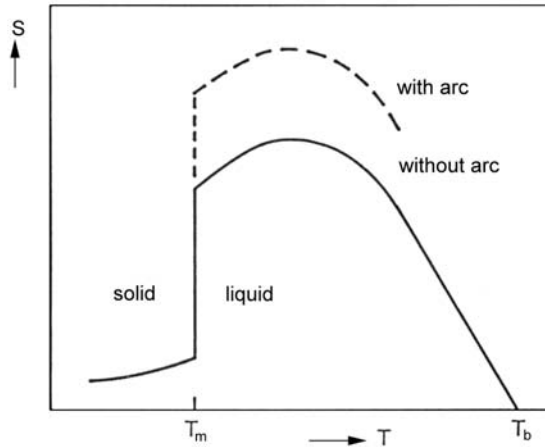


Figure 3.10. Solubility S of a di-atomic gas G_2 in a metal as a function of temperature.
 T_m = melting point, T_b = boiling point.

Because of the dynamic character of the welding process, the interaction between di-atomic gases and the liquid metal of the weld pool during fusion welding rarely results in an equilibrium situation. The deviation from equilibrium is particularly apparent in the case of arc welding. The results of experiments show that under arc welding conditions (in the presence of an arc), substantially more gas is absorbed by the liquid metal than predicted by Sieverts' law. This is illustrated by Figure 3.11, in which the concentration of absorbed nitrogen $[N]$ is plotted as a function of $\sqrt{\%N_2}$ in the case of arc welding of steel. For comparison the figure also shows the nitrogen concentration predicted by Sieverts' law (non-arc conditions). See also the dotted line in Figure 3.10.

The enhanced gas absorption observed in the case of arc welding is caused by the high degree of dissociation of the di-atomic gas due to the high arc temperature. This results in a high concentration of gas atoms, which facilitates the absorption at the metal surface.

In Figure 3.12 the gas concentration $[G]$ in the weld metal during welding is schematically presented as a function of time. The figure shows that the gas concentration increases during heating of the liquid metal and decreases during cooling. Usually, the gas concentration remains above the solubility during the lifespan of the weld pool, which may result in the nucleation and growth of gas bubbles. Bubble formation can also take place during solidification. Due to the downward jump of the solubility at the solidification temperature, gas will be rejected from the solidifying metal, which results in a surplus of gas ahead of the solidification front. Consequently, the gas concentration ahead of this front will rise and eventually will exceed the solubility of the gas at that temperature, which may

lead to the nucleation and growth of gas bubbles. When the bubbles are sufficiently large, they will try to escape to the surface. Bubble formation leads to porosity when the bubbles are caught up by the moving solidification front.

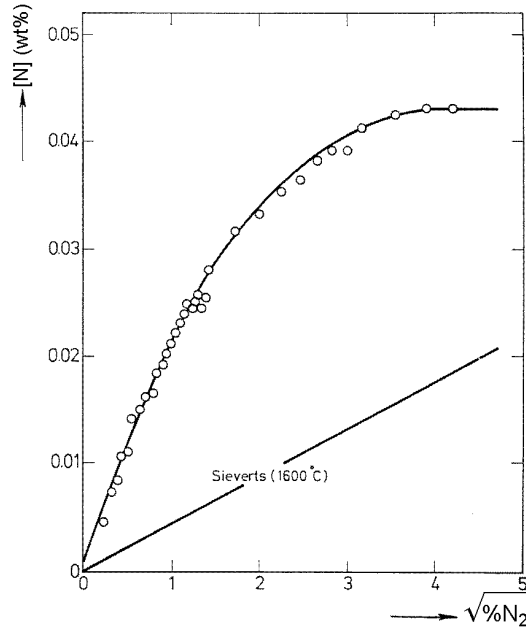


Figure 3.11. The concentration of absorbed nitrogen $[N]$ as a function of $\sqrt{\%N_2}$ in the case of arc welding of steel.

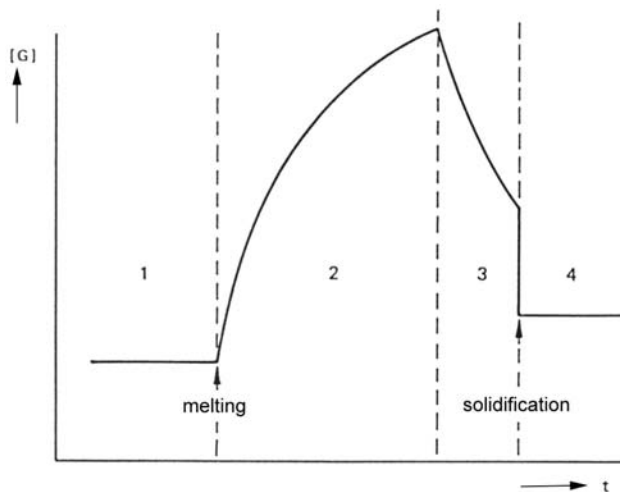


Figure 3.12. Schematic representation of the gas concentration $[G]$ in the weld metal during welding as a function of time: 1) heating of the solid metal; 2) heating of the liquid metal; 3) cooling of the liquid metal; 4) solidification and cooling of the solidified material.

3.5 Structure of the welded joint

Microscopic examination shows that different regions can be distinguished in a fusion weld, each characterized by its own macro- and microstructure. These regions are schematically represented in Figure 3.13 and are described in the following.

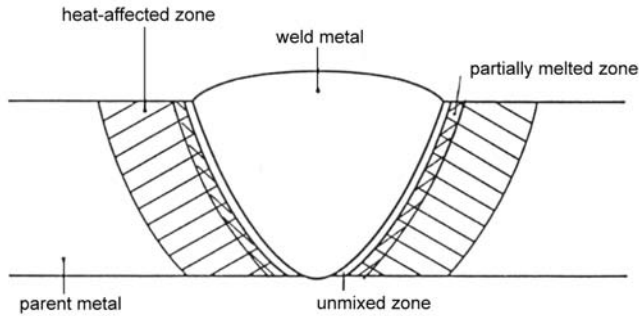


Figure 3.13. Schematic representation of the different regions in a fusion weld.

3.5.1 Weld metal

Weld metal is the metal that melted during the welding process and solidified after passage of the heat source. Weld metal has the chemical composition of the parent metal in the case of welding without the use of consumable material (electrode, filler wire or powder), and a mixed composition determined by the mixing parameter when welding with consumable material (see Section 3.2). In weld metal, a distinction can be made between the primary, the secondary and the tertiary structure.

The *primary structure* is the structure formed immediately after solidification. Solidification of the weld metal generally follows the standard theories, with distinct features related to the specific welding conditions.

The primary structure is a casting structure, consisting of columnar crystals, and is characterized by:

- epitaxial growth, the columnar grains are nucleated at the solid grains at the fusion boundary and grow toward the weld centreline, preserving the same crystallographic orientation as the nucleating grains;
- a growth direction perpendicular to the solid/liquid interface, which is the direction of the maximum temperature gradient (maximum heat transfer);
- a preference for growth in a specific direction (the $\langle 100 \rangle$ direction in cubic metals and the $\langle 1010 \rangle$ direction in hexagonal close-packed metals); grains growing in the preferred direction proceed more easily and crowd out grains growing in a deviating direction (competitive growth), resulting in texture.

In Figure 3.14 the primary structure of a single-pass arc weld is schematically presented in the form of three cross-sectional views.

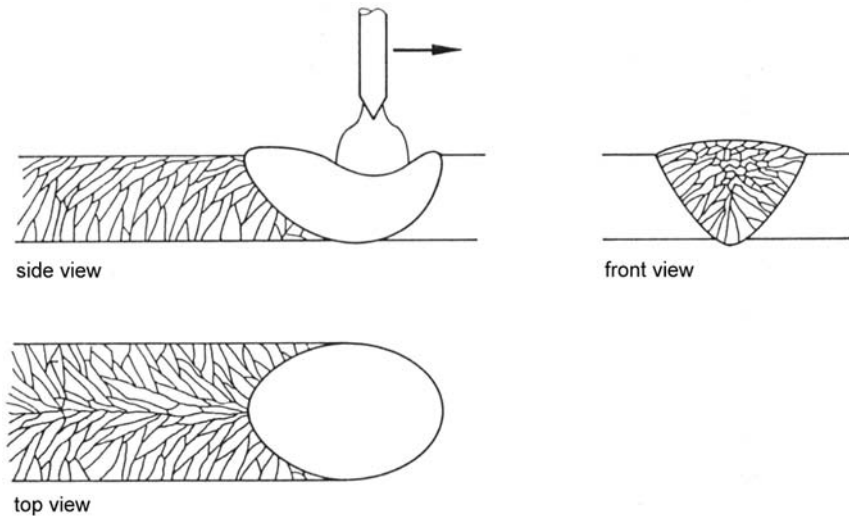


Figure 3.14. Primary structure of a single-pass weld.

It has already been shown in Section 3.2 that the shape of the weld pool depends on the travel speed: the larger the travel speed, the more elongated the weld pool. As the columnar grains grow in a direction perpendicular to the fusion boundary, this implies that also the primary structure of the weld depends on the travel speed. This is illustrated in Figure 3.15, which depicts the primary structure in top view for two situations: an elliptical weld pool (relatively low travel speed) and a tear-shaped weld pool (relatively high travel speed).

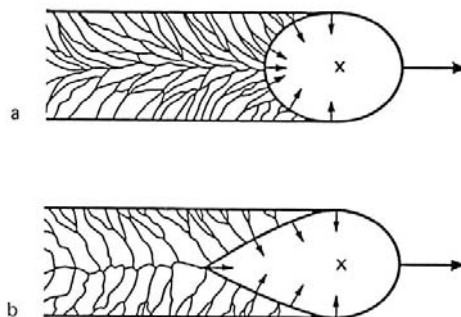


Figure 3.15. Top view of the primary structure, a) elliptical weld pool and b) tear-shaped weld pool.

In the case of an elliptical weld pool the direction of the maximum temperature gradient does change over time. Favourably oriented grains will gradually become

less favourable and will eventually stop growing, making it possible for other grains to nucleate and grow.

In the case of a tear-shaped weld pool the direction of the maximum temperature gradient does not (or only slightly) change when the solidification progresses. Consequently, the grains can grow out to a considerable size and, advancing from both sides, will meet at the centreline.

In addition to the columnar grains shown in Figure 3.15, sometimes axial grains running parallel to the weld centreline can be observed. This occurs especially at low travel speed.

At high travel speed heterogeneous nucleation can take place at the weld centreline, resulting in a narrow band of equi-axed grains.

The primary structure of a weld can be refined by means of ultrasonic vibration or by adding grain refining substances to the weld pool. In the case of arc welding use can also be made of arc oscillation or electro-magnetic stirring of the weld pool.

Microscopic examination of fusion welds shows that the columnar grains of the primary structure usually have a substructure, which depends on different factors, notably the chemical composition of the liquid weld metal and the welding parameters. The formation of this substructure is directly related to the occurrence of constitutional supercooling during the solidification and will be described with the help of Figure 3.16 in the case of welding an alloy, in which an alloying element of nominal concentration c_0 is dissolved.

During welding of this alloy, the solidification front will move with a certain uniform speed, as indicated in Figure 3.16a. Because the solubility of the alloying element is smaller in the solid metal than in the liquid metal, solute atoms will be pushed from the solid to the liquid, which will result in an enrichment of the alloying element in the liquid in front of the solid/liquid interface. This enrichment will be opposed by diffusion of the alloying element in the liquid metal. A stationary situation will be established, when the amount of alloying element pushed from the solid into the liquid metal per unit time, is equal to the amount transferred per unit time by diffusion, assuming that flow of the liquid metal along the solidification front can be neglected. The concentration of the alloying element in the liquid metal as a function of the distance to the solid/liquid interface is shown schematically in Figure 3.16b. For equilibrium, expressed by the hypothetical phase diagram depicted in Figure 3.16c, it is assumed that diffusion in the solid is not limited. In the practice of welding, however, the cooling rate is high and diffusion in the solid plays a minor role, which will result in segregation.

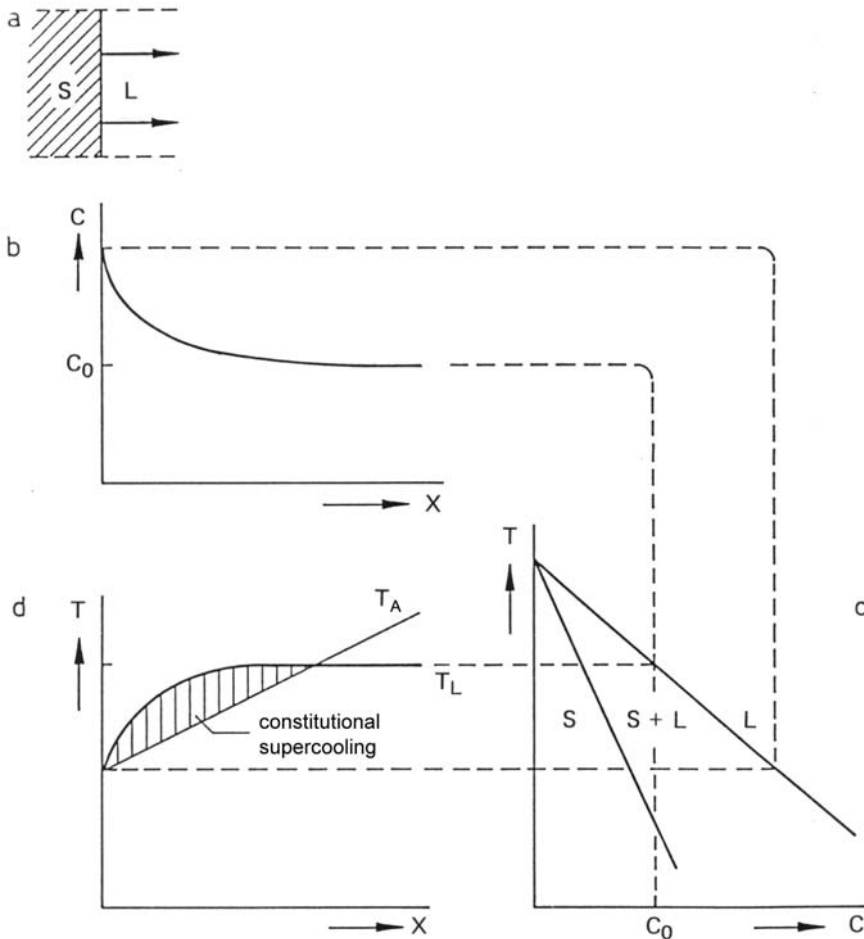


Figure 3.16. Constitutional supercooling.

The increase in concentration of the alloying element in front of the solid/liquid interface results in a decrease of the liquidus temperature T_L . The value of T_L as function of the distance to the solid/liquid interface can be obtained by combining Figure 3.16b with the phase diagram. The result is shown in Figure 3.16d, in which in addition to the liquidus temperature T_L also the actual temperature T_A is plotted as function of the distance to the solid/liquid interface.

As indicated by the dashed region in this figure, constitutional supercooling occurs when

$$T_L > T_A.$$

Figure 3.16d also shows that constitutional supercooling is promoted by:

- increasing the concentration gradient in the liquid metal in front of the solidification front, i.e. by increasing the solidification rate;
- reducing the temperature gradient in the liquid metal in front of the solid/liquid interface.

As a result of constitutional supercooling, different substructures may be formed within the primary grains of the weld metal. A distinction can be made between flat, cellular, cellular-dendritic and dendritic substructures. These substructures are shown schematically in Figure 3.17.

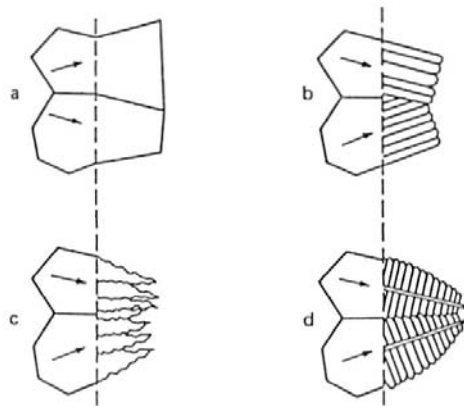


Figure 3.17. Different substructures of weld metal: a) flat; b) cellular; c) cellular-dendritic; d) dendritic.

Which substructure will be formed in a specific situation depends on two factors: the chemical composition (concentration of alloying element) and the solidification rate. The solidification rate is usually expressed in terms of the solidification parameter G/R , where G is the temperature gradient at the solidification front and R the speed of the solidification front.

The influence of the chemical composition and the solidification parameter on the substructure are shown schematically in Figure 3.18.

Both G and R depend on the position on the solidification front. Generally, G has its minimum value at the centre of the solidification front, while R has at its maximum at that position.

More specifically, R can be expressed as:

$$R = v \cos \theta \quad (3.21)$$

where v is the travel speed and θ the angle between the travel direction and the solidification direction. This is illustrated in Figure 3.19.

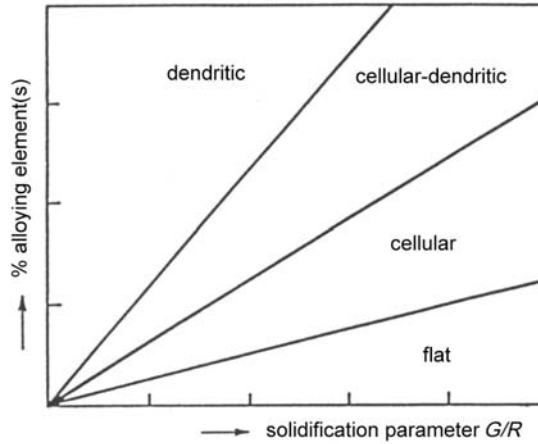


Figure 3.18. Schematic representation of the influence of the chemical composition and the solidification parameter on the substructure of weld metal.

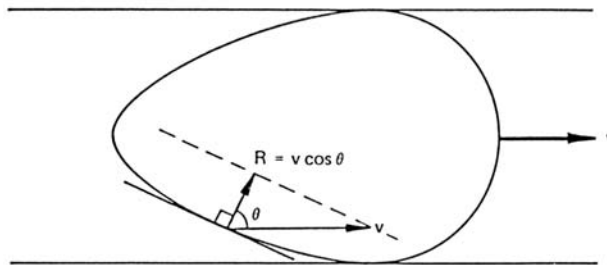


Figure 3.19. The speed R of the solidification front as a function of the position on this front.

In the case of weld metal characterized by a phase transformation in the solid state, the primary structure formed immediately after solidification will undergo a drastic change when during cooling of the weld the transformation temperature is passed. The newly formed structure consists of transformation products and is often referred to as *secondary structure*.

It is evident that the substructure formed in the primary grains during solidification is destroyed by the phase transformation. However, due to the fact that the nucleation of the transformation products starts at the grain boundaries of the original primary grains, the primary structure usually remains recognizable. A typical example of the secondary structure is the room temperature microstructure observed in the case of low-alloy steel weld metal. This structure consists of grain boundary ferrite, side-plate ferrite, acicular ferrite and bainite, formed during the austenite-ferrite phase transformation, in quantities depending on the chemical composition and the cooling rate (see Section 4.3).

The *tertiary structure* is formed in the case of multi-pass welding. Due to the deposition of each welding pass, the preceding pass will be subjected to a reheat treatment, resulting in recrystallization and grain growth. The tertiary structure therefore consists of equi-axed grains, which increase in size with increasing reheat temperature.

3.5.2 The unmixed zone

This zone is the outermost layer of the weld metal. It typically has a thickness of tenths of millimetres. The metal in this zone melted but did not mix with the rest of the liquid metal in the weld pool during the welding process. The unmixed zone therefore has the structure of the weld metal, but the chemical composition of the parent metal. Although always present, this zone is especially apparent in the case of welding with consumable material (electrode, filler wire or powder) having a chemical composition, which differs significantly from that of the parent material.

3.5.3 The partially melted zone

A characteristic feature of alloys is that they have a melting range rather than a melting point. This implies that when welding an alloy, partial melting takes place in a narrow zone adjacent to the solid parent metal. The zone in which partial melting takes place is called the partially melted zone or mushy zone and is shown schematically in Figure 3.20.

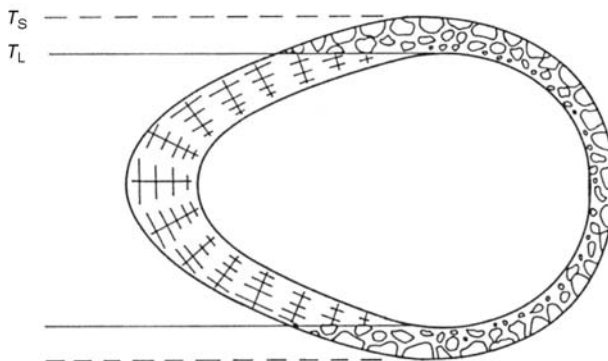


Figure 3.20. Schematic representation of the partially melted zone.

The width of the partially melted zone is determined by the size of the melting range. The fraction of liquid metal in this zone depends on the local temperature gradient and varies from 0% at the dotted line (solidus temperature T_S) to 100% at the edge of the weld pool (liquidus temperature T_L). Melting occurs particularly along grain boundaries and to a lesser extent in the interior of the grains.

The partially melted zone of a weld can give rise to severe problems, the most important being hot cracking (see Section 3.8).

3.5.4 The heat-affected zone

The heat-affected zone of a weld is defined as the zone of the parent metal adjacent to the weld metal, which did not melt, but was subjected to a thermal cycle caused by the welding process. The thermal cycle due to welding has been discussed in Section 3.1.

Evidently, this thermal cycle will influence the microstructure and the properties of the metal in the heat-affected zone. Which microstructural changes occur in a specific case, depends on the metal in question and on the thermal cycle experienced (i.e. on the distance from the fusion boundary). Especially the peak temperature and the cooling rate play an important role. Examples of microstructural changes that may occur in the heat-affected zone are given below.

– *Grain growth*

This phenomenon occurs in almost all metals and alloys and becomes more prevalent as the temperature increases. It results in the formation of a coarse-grained subzone directly adjacent to the fusion boundary. The driving force of grain growth is the reduction of interfacial energy. This will affect solid state transformations and thus the development of the microstructure upon cooling, as the number of nucleation sites (mainly at the grain boundaries) is reduced.

– *Formation of new phases*

In the case of metals and alloys characterized by a phase transformation in the solid state, new phases may be formed in the heat-affected zone. This can either be phases, which are formed under more or less equilibrium conditions so that phase diagrams can be used or phases that will be formed under non-equilibrium conditions (at high cooling rate). A well-known example is the formation of martensite when welding carbon steels.

– *Strain ageing*

When nitrogen containing steel is strained and subsequently heated to a temperature of a few hundred degrees, FeN precipitates will cluster around dislocations, which results in precipitation embrittlement and loss of ductility. This phenomenon is called strain ageing and can easily occur in the heat-affected zone.

– *Over-ageing*

Some alloys (notably the heat-treatable aluminium alloys) derive their strength from precipitation hardening (solution heat treatment and quenching followed by either natural or artificial ageing, which produces a fine dispersion of the strengthening precipitates). When these alloys are welded, over-ageing may occur in the heat-affected zone. Over-ageing results in an increase of the size of the

precipitates at the cost of their number, which in turn causes a reduction in strength.

– *Annealing of work hardening*

The strength of metals and alloys can be increased by work hardening, such as rolling, extruding or forging. When work-hardened alloys are welded, the heat-affected zone may be fully or partly annealed, thus irreversibly reducing its strength.

In the case of welding processes, which rely on plastic deformation, as for instance friction stir welding, annealing may have a beneficial effect on the heat-affected zone.

– *Weld decay*

When welding certain types of stainless steel, depletion of chromium along the grain boundaries in the heat-affected zone may take place. This phenomenon (weld decay) results in a reduction of the corrosion resistance.

Some of the phenomena mentioned in the foregoing will be discussed in more detail in the following chapters.

3.6 Residual stresses and distortion

Due to the non-homogeneous heating and cooling of the workpiece during welding, residual stresses will be introduced into the workpiece, which may lead to plastic deformation and distortion. Residual stresses and distortion of the workpiece are closely related. Generally speaking, minimizing the distortion of the workpiece, for instance by a clamping device, will result in an increase of the residual stresses. This trend is schematically depicted in Figure 3.21.

Residual stresses originate primarily from differences in thermal expansion and shrinkage in the weld zone and the surrounding metal. Therefore, these stresses are also referred to as thermal stresses.

As long as the stresses remain elastic, the workpiece will return to its original shape upon cooling and no distortion is introduced. However, in fusion welding this situation is unlikely to happen, as major differences in temperature will locally result in plastic deformation.

It should be noted that most mechanical properties of materials are temperature dependent. In fact the yield strength and the modulus of elasticity decrease significantly with increasing temperature. Therefore, plastic deformation during fusion welding will in particular occur in the hotter regions.

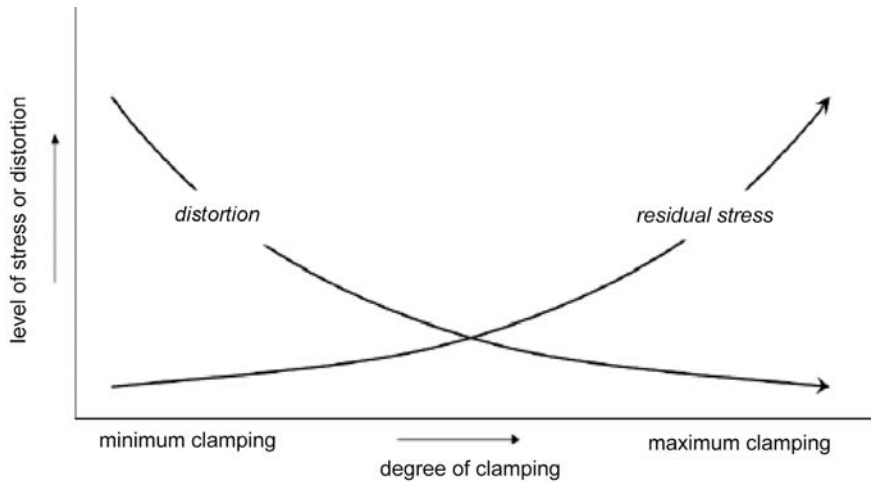


Figure 3.21. Relation between stress and distortion.

A second source of residual stresses are microstructural transformations, which may occur during welding. Microstructural transformations generally involve changes in specific volume. For instance, the transformation of austenite to ferrite in steel is accompanied by an expansion of 1.03 vol. %, whereas transformations to upper bainite, lower bainite and martensite result in volumetric changes of 4.22, 4.36 and 4.53 vol. % respectively.

Residual stresses are internal stresses, i.e. the stresses are not due to external forces. Therefore, the stresses have to be in equilibrium. This means that tensile stresses in a specific part of the workpiece have to be compensated by compressive stresses in other parts. The transient behaviour of stresses during the whole thermal cycle of welding implies that a self-equilibrium is maintained during the course of welding.

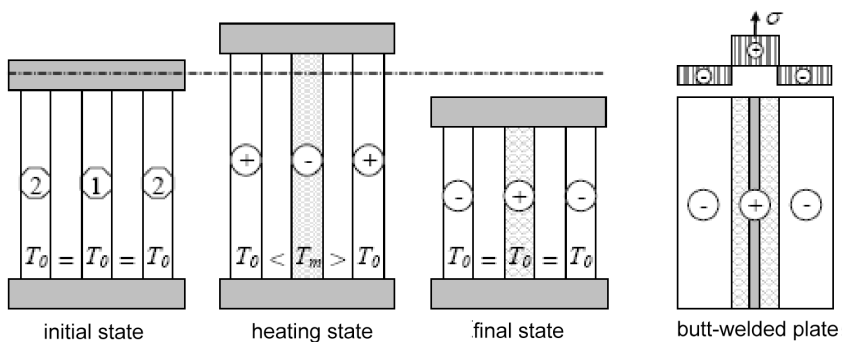


Figure 3.22. Three-bar system representing a butt-weld in a rectangular plate.

The transient development of stresses due to localised heating can be described by a simple three-bar model schematically depicted in Figure 3.22. In this model the

workpiece is represented by three bars: the middle bar (bar 1) representing the hot weld area and two outer bars (bars 2), representing the cold unaffected base material. The three bars are rigidly interconnected. When the temperature of the middle bar increases, the bar will expand. This expansion is restrained by the outer bars, which remain at ambient temperature. Due to this restraint, compressive stresses are generated in the middle bar. Initially, the stress is elastic. However, when the stress in the middle bar reaches the yield stress it will deform plastically. It should be noted that as a result of the increase in temperature the yield stress decreases. This implies that the stress in the bar will follow the yield stress versus temperature curve. Upon cooling the process is reversed: tensile stresses develop in the middle bar due to the constrained contraction and balancing stresses develop in the outer bars. After the full thermal cycle, the middle bar experiences a tensile stress and the outer bars are in a balancing compressive stress state. This situation resembles the situation of a butt-weld in a rectangular plate.

Obviously, the above described evolution of stresses based on the three-bar model is a simplification of the actual situation during welding. More realistic results are obtained when a more precise temperature distribution is used and also the stress reset due to melting and the volume changes due to phase transformations are taken into account.

A typical stress distribution around a single-pass weld in a rectangular plate is shown in Figure 3.23.

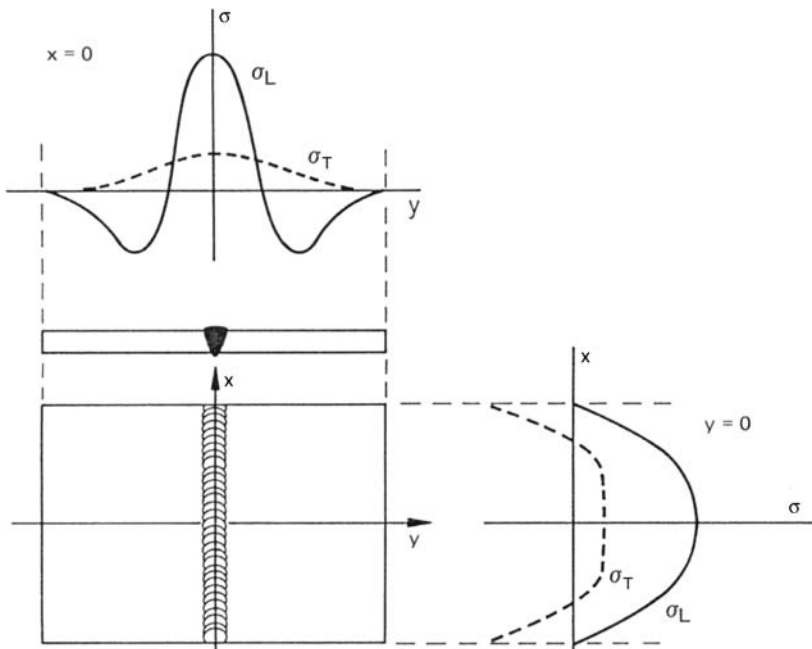


Figure 3.23. Stress distribution around a single-pass weld in a rectangular plate.

The figure shows that the longitudinal stress σ_L (the stress parallel to the weld) is tensile in the weld and becomes compressive at increasing distance from the weld centre line (equilibrium requires that $\int \sigma_L dy = 0$). In the x-direction the longitudinal stress σ_L decreases to zero at the plate edges.

The transversal stress σ_T (the stress perpendicular to the weld) is a tensile stress, which decreases with increasing distance from the weld to zero at the edges of the plate. In the x-direction σ_T changes from a tensile to a compressive stress (equilibrium requires that $\int \sigma_T dx = 0$).

Residual stresses have a negative influence on the integrity of the welded joint. Firstly, they promote weld cracking, in particular hot cracking, fatigue-induced cracking and stress corrosion cracking. In addition, they may cause distortion of the workpiece.

As an illustration Figure 3.24 shows the different distortions, which may be observed in the case of welding two metal plates:

- transverse shrinkage
- longitudinal shrinkage
- rotational distortion
- angular distortion
- bending distortion
- buckling.

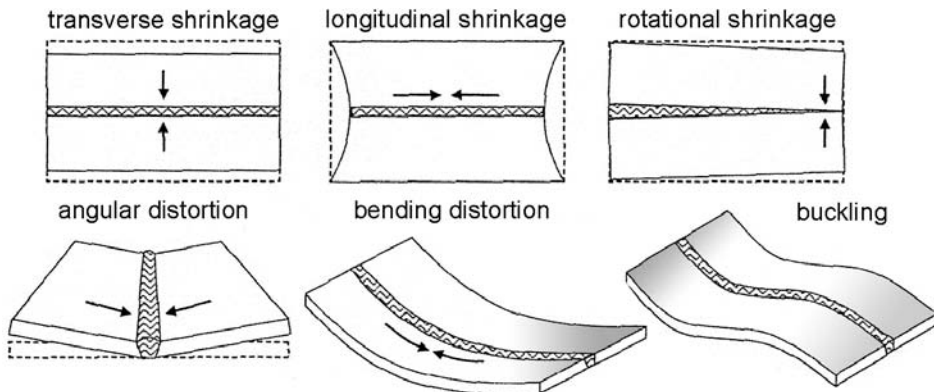


Figure 3.24. Distortions caused by residual stresses in the case of welding two plates (V-groove, free support). After Masubuchi, 1980.

The development of residual stresses can be counteracted in a number of ways. Firstly, the material to be welded can be pre-heated. Pre-heating results in a reduction of the cooling rate and of the temperature gradient in the workpiece and, hence, to a reduction of residual stress.

After welding the level of residual stresses can be reduced by post-weld heat treatment and by mechanical treatment (hammering, peening, vibrating).

Minimizing the level of residual stresses also requires a correct choice of the welding procedure. This is illustrated with the following examples.

– *Tack welding*

Tack welding is used to fix the position of two or more metal part, which are to be joined by welding. The incorrect and the correct way of tack welding are shown schematically in Figure 3.25.

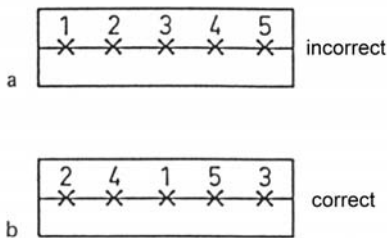


Figure 3.25. Tack welding. The numbers indicate the sequence of welding.

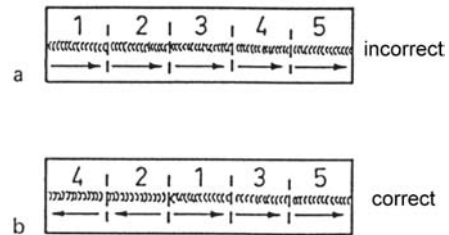


Figure 3.26. Deposition of long welds. The numbers indicate the sequence of welding.

– *Deposition of long welds*

Welds of great length are usually deposited by serial welding of small sections rather than by welding in one run. The incorrect and the correct way of welding are shown schematically in Figure 3.26.

– *Multi-pass welding*

In the case of multi-pass welding the inter-pass temperature (the temperature to which the workpiece is cooled before the next pass is deposited) should be carefully chosen as this temperature has an important effect on the development of residual stresses: the lower the inter-pass temperature the higher the stress level.

Different methods are available to measure residual stresses in welded materials, the most important being:

- X-ray diffraction techniques: stress levels in the material are determined by measuring the broadening and shift of diffraction peaks, as stresses affect the lattice spacing;
- Stress relaxation techniques: localised removal of stressed material results in strain relief in the adjacent material, which can be measured for instance by strain gauges.

3.7 Weld defects

During fusion welding different weld defects can be formed, which under specific conditions may impair the integrity and reliability of the welded joint. The most important weld defects are: cracks, pores, inclusions, lack of fusion, insufficient weld penetration and undercut, see Figure 3.27.

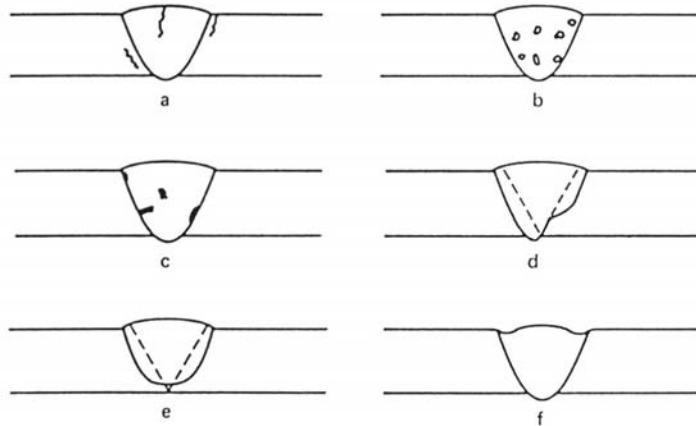


Figure 3.27. Weld defects: a) cracks; b) pores; c) inclusions; d) lack of fusion; e) insufficient weld penetration f) undercut.

Cracks are by far the most dangerous weld defects. They also differ from the other defects in that they are metallurgical in nature. In view of this, cracks will be discussed separately in Section 3.8, whereas the other defects will be briefly described below.

– Pores

Pores are gas cavities, formed in the weld metal during the welding process. In most cases, pore formation is due to the absorption by the liquid weld metal of diatomic gases, such as nitrogen or hydrogen, from the surrounding atmosphere. Gases can also be produced in the liquid weld metal itself by chemical reactions. For instance, in the case of welding carbon steel, oxidation of carbon may result in the formation of carbon monoxide. Under specific conditions the gas concentration in the liquid metal increases to a level, which exceeds the solubility limit. This may result in the nucleation and growth of gas bubbles during cooling and solidification of the liquid weld metal. When the gas bubbles are sufficiently large, they will try to escape to the surface. Bubble formation leads to porosity when the bubbles are caught up by the moving solidification front. The pores are usually spherical, but under specific circumstances long pores ('worm holes') may be formed.

– *Inclusions*

When slag plays a role in the welding process (as, for instance, in the case of MMA welding, GMA welding with flux-cored wire and SA welding), slag inclusions may enter the liquid weld metal. Most slag types float on top of the liquid weld metal because of their lower density. However, due to turbulent movement of the liquid weld metal some of the slag may be trapped inside the weld pool in the form of inclusions. Usually, these inclusions have an irregular shape and are randomly distributed in the weld, sometimes they form a continuous or discontinuous array in the direction of welding.

In the case of GTA welding, melting or crumbling of the electrode can cause tungsten or tungsten oxide to enter the weld pool. Upon solidification, this tungsten remains in the weld metal in the form of tungsten(oxide) inclusions.

– *Lack of fusion*

Lack of fusion is a weld discontinuity, which may occur during fusion welding when liquid weld metal comes into contact with unmolten parent metal. This results in an area with insufficient binding between weld metal and parent metal. In most cases lack of fusion is caused by the presence of oxides or other surface layers on the parent metal.

Lack of fusion can also occur between subsequent weld layers in the case of multi-pass welding.

- *Insufficient weld penetration*

The weld penetration depth is one of the geometric parameters that define weld quality. Insufficient penetration occurs when the weld metal does not extend through the joint thickness.

In most cases insufficient penetration is caused by the choice of an incorrect joint design and/or by using incorrect welding parameters.

- *Undercut*

Undercut is a weld defect occurring at the edge of the weld metal. At this location the weld groove is not completely filled, leaving a discontinuity at the boundary between the weld metal and the heat-affected zone. This discontinuity may have a smooth shape, but is usually sharp.

Generally speaking, the weld defects briefly described above have a negative effect on the mechanical properties of the welded joint. This is in particular the case when the defects are flat and/or sharp. The negative influence of the round/spatial weld defects (i.e. pores) is usually limited to a decrease of the static mechanical properties, proportional to the reduction of the (effective) area of the weld cross-section.

In most cases the formation of these weld defects can be avoided by a correct choice of the welding procedure and accurate groove preparation.

Numerous non-destructive testing (NDT) methods exist to detect and identify weld defects. The most important NDT methods are reviewed in Chapter 7.

3.8 Hot cracking

As stated earlier, cracks are by far the most dangerous weld defects. Different crack types can be distinguished: hot cracks, cold cracks, reheat cracks and lamellar cracks. Hot cracking relies on the presence of a melting/solidification range and therefore may occur in practically all alloys, whereas the other crack forming mechanisms exclusively occur in ferritic steel.

Because of its general nature, only hot cracking will be considered in this section. Cold cracking, reheat cracking and lamellar tearing will be addressed in Chapter 4, which deals with welding of ferritic steel.

Hot cracks are formed at high temperature, usually several hundred degrees below the melting point or the solidus temperature of the alloy.

They do not only form during fusion welding, but can also form during casting or hot forming. The cracks propagate intergranularly (i.e., along the grain boundaries). Two types of hot cracks may be distinguished: solidification cracks and liquation cracks.

Solidification cracking may occur in weld metal characterized by a melting/solidification range. Cracking takes place in the final stage of the solidification process at a temperature near the solidus temperature. In this stage, the primary dendrites/columnar grains that grow into the molten metal from both sides of the weld pool, meet. This creates a coherent network, which will contract upon further cooling, leading to shrinkage stresses. Solidification cracking will occur when these stresses exceed a critical value. Whether cracks will form, depends mainly on the chemical composition of the weld metal.

In most cases solidification cracks are formed in the centre of the weld where the columnar grains meet (centreline cracks). A typical centreline crack is schematically shown in Figure 3.28.

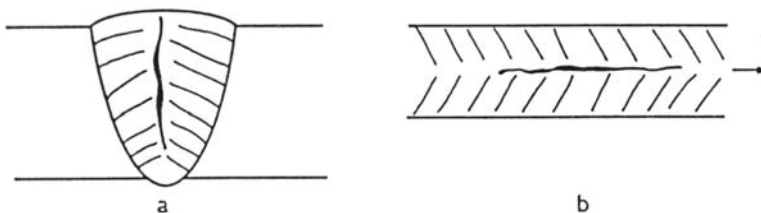


Figure 3.28. Schematic representation of a centreline crack in weld metal: a) transverse cross-section, b) top view.

If the crack forms in a stage where a relatively large quantity of liquid is still present, it can be annihilated by back-filling. This will especially occur in the case of alloys containing a high amount of eutectic liquid (eutectic healing).

Liquation cracking may occur in the heat-affected zone when a low-melting phase is present at the grain boundaries. During welding these phases may melt and depending on the surface tension may spread out as a film on the grain boundaries. In this way, the structure is weakened and stresses due to shrinkage may cause cracking. An example of a liquation crack in the heat-affected zone is shown in Figure 3.29.

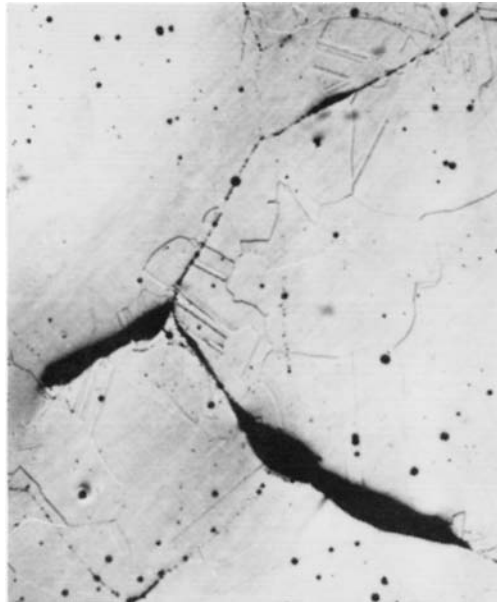


Figure 3.29. Liquation crack in the heat-affected zone.

The risk of hot cracking can be reduced by minimizing the restraint on the weld. This can be achieved by correct workpiece preparation, accurate fixing and choosing appropriate welding conditions.

3.9 Weldability

The term weldability is a qualitative term, which expresses the ease with which a metal may be welded. More precisely, this term is used to characterize the possibility to use a certain welding process to create a weld in a particular material suitable for a specific purpose.

Usually, a distinction is made between the *executive*, the *metallurgical* and the *constructive weldability*.

The *executive weldability* refers to the possibility to create a homogenous metallic

welded joint, in which no macroscopic defects or imperfections are present. This implies that a variety of welding tests must be performed when a new construction material or filler wire is to be used, or a new welding method is considered.

The *metallurgical weldability* refers to the necessity for the weld to have adequate mechanical properties), i.e. mechanical properties, which match the demands of the construction of which the weld is a part. The metallurgical weldability is largely determined by the influence of the welding process on the properties of the weld. Evidently, this influence is specific for the metal considered. For instance, when welding unalloyed steel, the heat-affected zone will usually have a lower ductility than the parent metal, whereas in the case of welding stainless steel, a reduction of corrosion resistance in the region around the weld may be observed.

The *constructive weldability* refers to the capability of the welded construction to withstand degradation under service conditions. This means that the construction must be able to endure the stresses, which develop during use of the construction. Insufficient constructive weldability would possibly lead to the initiation and/or propagation of cracks.

In the past a variety of techniques have been developed to test the weldability of metallic materials. Most of these techniques address a specific aspect of the weldability.

The following techniques are used to test the weldability: hardness measurements, tensile tests, bending tests, impact tests, CTOD (Crack Tip Opening Displacement) measurements, fatigue tests, corrosion resistance tests and a number of crack-sensitivity tests, of which the vareststraint-test (hot cracking) and the implant test (cold cracking) are the best known.

The different weldability tests will not be discussed here. The reader is referred to the literature.

Bibliography

- [3.1] Cerjak, H. and Easterling, K.E., *Mathematical modelling of weld phenomena*, The Institute of Materials, London, 1993.
- [3.2] Davies, A.C., *The science and practice of welding*, 8th Edition, Cambridge University Press, Cambridge, 1986.
- [3.3] Easterling, K.E., *Introduction to the Physical Metallurgy of Welding*, Butterworths & Co., London, 1983.
- [3.4] Granjon, H., *Fundamentals of Welding Metallurgy*, Woodhead Publishing Ltd, Cambridge, 1991.
- [3.5] Grong, O., *Metallurgical Modelling of Welding*, The Institute of Materials, London, 1994.
- [3.6] Houldcroft, P. and John, R., *Welding and Cutting*, Woodhead-Faulkner, London, 1988.
- [3.7] Kou, S., *Welding Metallurgy*, John Wiley & Sons, New York, 1987.
- [3.8] Lancaster, J.F., *Metallurgy of Welding*, 4th Edition, George Allen & Unwin, London, 1987.
- [3.9] Masubuchi, K., *Analysis of welded structures*, Pergamon Press, Oxford, 1980.
- [3.10] Metals Handbook, 9th Edition, Vol. 6: *Welding, brazing and soldering*, American Society for Metals, Cleveland, 1983.

- [3.11] Nguyen, N.T., *Thermal analysis of welds*, WIT Press, Southampton, 2004
- [3.12] Radaj, D., *Welding residual stresses and distortion*, DVS-Verlag, 2003.
- [3.13] Rykalin, N.N., *Calculation of heat flow in welding*, Document 212-350-74, International Institute of Welding, London, 1974.
- [3.14] *Welding Handbook*, 8th Edition, Vol. 1: *Welding Technology*, American Welding Society, Miami, 1987.